JACS
JOURNAL OF THE AMERICAN CHEMICAL SOCIETY
Article
pubs.acs.org/JACS

# CO Self-Promoting Oxidation on Nanosized Gold Clusters: Triangular $Au_3$ Active Site and CO Induced O−O Scission

Chunyan Liu,[†] Yingzi Tan,[†] Sisi Lin,[†] Hui Li,[‡] Xiaojun Wu,[§] Lei Li,[‡] Yong Pei,*[,†] and Xiao Cheng Zeng*[,‡]

[†]Department of Chemistry, Key Laboratory of Environmentally Friendly Chemistry and Applications of Ministry of Education, Xiangtan University, Hunan Province 411105, People's Republic of China

[‡]Department of Chemistry and Nebraska Center for Materials and Nanoscience, University of Nebraska—Lincoln, Lincoln, Nebraska 68588, United States

[§]CAS Key Laboratory of Materials for Energy Conversion and Department of Material Science and Engineering, University of Science and Technology of China, Hefei, Anhui 230026, People's Republic of China

Supporting Information

**ABSTRACT:** We have systematically studied the CO oxidation on various nanosized gold clusters with sizes ranging from 0.3 to 0.8 nm on the basis of density functional theory (DFT) calculations. A hitherto unreported trimolecular Langmuir-Hinshelwood (LH) mechanism is proposed, which offers new insights into the fundamental mechanism for CO oxidation on nanosized gold clusters. Specifically, we find that the coadsorbed CO molecule at a unique triangular $Au_3$ active site can act as a promoter for the scission of an O−O bond, leading to the spontaneous formation (due to extremely low energy barrier) of two $CO_2$ molecules as product. The key step to the O−O bond scission in the OCOO* intermediate is significantly accelerated due to the electrophilic attack of the coadsorbed neighboring CO molecule on the triangular $Au_3$ site. This new mechanism is called CO self-promoting oxidation, which can be visualized in real time from the trajectory of a Born−Oppenheimer molecular dynamics (BOMD) simulation. We also find that such CO self-promoting oxidation is quite universal, as long as the triangular $Au_3$ reaction site is available. This is demonstrated in two prototype metal oxide supported gold nanostructure systems: namely, $Au_n$/MgO and bilayer-Au/$TiO_2$. The coadsorbed CO can not only serve as a promoter for its own oxidation but also promote other oxidation reactions such as styrene oxidation through expediting O−O scission on gold nanostructures.

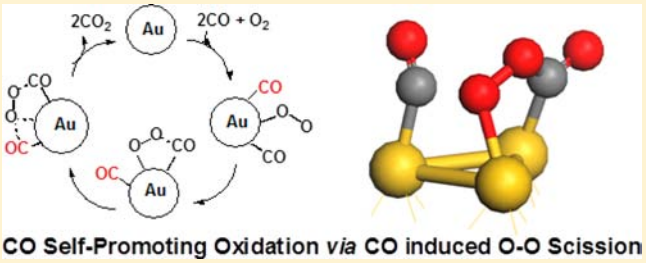


## 1. INTRODUCTION

Nanosized gold clusters have attracted great interest over the past few decades owing to their unusual catalytic properties not seen in bulk gold. For example, nanosized gold clusters exhibit high catalytic activities toward carbon monoxide oxidation,[1] selective oxidation of olefin and alcohol,[2,3] and synthesis of hydrogen peroxide,[4] as well as toward the water-gas shift reaction.[5] Among various reactions catalyzed by gold clusters, CO oxidation has received the most attention and it has become a benchmark for examining activities of nanogold.[6−17] It has been well established from both gas-phase and supported gold cluster experiments that gold nanoparticles can catalyze the CO oxidation even below room temperature, a novel property that can be utilized to overcome the "cold start-up" problem known with the conventional Pt- and Pd-based catalysts.

Numerous experimental studies have also shown that the catalytic activities of nanosized gold clusters are size-dependent.[18−29] Au clusters with diameters in the range 0.5−3 nm are found to be more reactive than those of larger size, and gold nanoparticles of size greater than 4 nm exhibit a notable decrease in catalytic activity. Moreover, nanosized Au clusters supported on reducible oxide substrates such as $TiO_2$ and MgO surfaces yield enhanced catalytic activity for CO oxidation.[19,21−24] To date, a number of metal oxide supported Au catalysts have been developed for practical applications, such as high turnover frequencies, high selectivity and durability, and easy recoverability.[25−29] However, the active sites and reaction mechanisms of CO oxidation on nanogold catalysts remains controversial. Several studies suggested that the apparent catalytic activity of nanogold is due to the interplay among many factors, including particle size, electronic properties of the metal oxide support, preparation methods, etc. To confirm the catalytic nature of gold nanoclusters, a variety of unsupported gold nanostructures such as "naked" gold nanoparticules[30] and nanoporous gold (NPG)[31,32] have been prepared in the laboratory. All these unsupported gold nanostructures have been shown to be active

Received: September 24, 2012
Published: January 23, 2013

   dx.doi.org/10.1021/ja309460v | J. Am. Chem. Soc. 2013, 135, 2583−2595

in catalyzing different oxidation reactions, including CO oxidation.[33]

Theoretical calculations based on density functional theory (DFT) have played an important role in the exploration of the active site and chemical mechanism for the CO oxidation on gold nanostructures.[34−46] Thus far, the predicted active sites for the CO oxidations on oxide supported gold clusters can be loosely classified into two categories: (1) active sites on the gold nanocluster where CO and $O_2$ are adsorbed and react and (2) the perimeter interface between the Au cluster and the metal oxide support. The reaction pathway for CO oxidation on gold clusters has been commonly described by the bimolecular Langmuir−Hinshelwood mechanism, which involves the formation of an OCOO* intermediate first, followed by the breaking of an O−O bond, as shown in Scheme 1a.

**Scheme 1. Catalytic Cycle of Two Proposed Oxidation Mechanisms: (a) Conventional Bimolecular LH Mechanism and (b) Trimolecular LH Mechanism Involving CO Self-Promoting Oxidation**

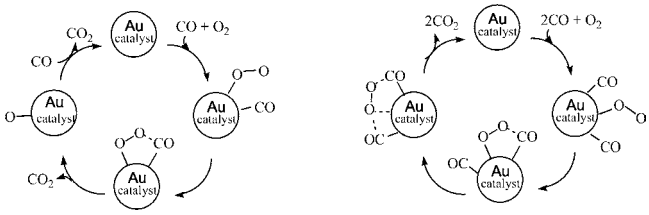


Within the framework of the bimolecular LH mechanism, several factors have been identified to account for the high activities of the nanosized gold clusters, which include low-coordination Au atoms on the surface of gold clusters, electron transfer between the cluster and support, the interface between Au and the oxide support, the magic number of electrons, the quantum effect of clusters, the structural fluxionality of gold clusters, the water moisture, the heteroatom dopant, etc.[34−46] In particular, the presence of water moisture and reducible metal oxide support have been demonstrated to notably promote CO oxidation. The mechanism underlying these promotion effects has been studied theoretically, and it is believed that the key step of $O_2$ adsorption and activation is actually promoted by either water moisture or the reducible oxide support.[36] However, few studies have taken into account the role of coadsorbed CO molecules during CO oxidation,[42−44] although many experimental and theoretical studies have shown the presence of multiple adsorbed CO molecules on the active sites of gold clusters, especially at relatively low temperature and elevated CO pressure.[47−54] Wallace et al., Veldeman et al., and Fielicke et al. reported the size- and pressure-dependent saturation adsorption of CO on both anionic and neutral gold clusters,[47−50] and all three groups found that the saturation ratio between CO and Au is close to 1 for Au clusters with up to 13 atoms. Mass spectrometry experiments and DFT calculations showed that the adsorption of CO and $O_2$ on the surface of gold clusters is cooperative, rather than competitive.[50−52] Gas-phase experiments combined with DFT calculations demonstrated that the chemisorption of several CO molecules on small gold cluster cations or anions ($Au_m(CO)_n^q$) can not only alter electronic properties of gold clusters but also significantly change the clusters' structure and reactivity toward the $O_2$ molecule.[55−59] In particular, recent gas-phase experimental studies indicate that the presence of multiadsorbed CO molecules affects the activity of gold clusters. Bürgel et al. found the CO oxidation is *self-promoted* on cationic gold oxide species.[60] Xie et al. found that neutral $Au_3(CO)_2$, $Au_5(CO)_4$, and $Au_7(CO)_5$ clusters are more reactive with $O_2$ than $Au_3(CO)_3$ and $Au_7(CO)_4$, although it is not clear whether the enhanced activity is due to the presence of multiadsorbed CO molecules.[61]

Apart from the gas-phase gold clusters, measurements of the rate of CO oxidation on oxide supported gold clusters indicated that the catalytic activity of Au nanoparticles not only is related to their ability to bind oxygen molecules but also depends on the CO partial pressure (order of reaction to CO is nonzero).[62] Gates et al. showed that the reaction rate of CO oxidation, catalyzed by $Au/CeO_2$ at 303 K, is proportional to $Pco^{0.19}$ and $P_{O_2}{}^{0.18}$ (where $P$ is the partial pressure).[63] Evidence of the nonzero order of the reaction associated with CO oxidation was also observed in several other experimental measurements.[62] Furthermore, comparative studies of the CO adsorption on Au nanocatalysts produced from different preparation methods confirmed the adsorption of multiple CO molecules on low-coordinated Au sites, especially on small gold clusters.[64−70]

Under the condition that multiple CO and $O_2$ molecules are coadsorbed around the active site on gold clusters, it is important to explore the extent to which the nearby adsorbed CO molecules can affect the CO oxidation. Would the coadsorbed CO molecules merely lead to certain electronic effects on the gold cluster, or would they actually be involved in the reaction? In a previous study of promotion effects due to water moisture, the mechanism proposed suggests that the water molecule can be coadsorbed on the neighboring site of preadsorbed CO and $O_2$ molecules,[36,40b] which first reacts with $O_2$ to produce a key $OOH^-$ intermediate, followed by promotion of the CO oxidation. Recently, a CO self-promoting oxidation mechanism on a single-crystal gold electrode in alkaline solution was uncovered such that the CO and $OH^-$ (oxidant) mutually enhance each other's binding on the electrode surface, thereby promoting CO oxidation.[71] Also, an unexpected promotion effect due to a coadsorbed CO molecule on the electrochemical oxidation of alcohol by $OH^-$ on gold was also reported recently.[72]

In this work, we carry out a comprehensive ab initio study of CO oxidation on a series of gold nanoclusters (with sizes ranging from 0.3 to 0.8 nm), and we propose a new trimolecular LH mechanism that offers new insights into the high activity of nanosized gold clusters toward CO oxidation. Specifically, we show that a coadsorbed CO molecule at the triangular $Au_3$ site can promote O−O bond breaking via a trimolecular LH mechanism (see Scheme 1b). Hereafter, we call this mechanism CO *self-promoting* oxidation. The paper is organized in two parts. The first is identification of the active site on nanosized gold clusters (with sizes 0.3−0.8 nm). To this end, we first investigate the oxidation path associated with a single CO on different sized gold clusters, ranging from two-dimensional (2D) flakes ($Au_7$−$Au_{10}$), to "flat cages" ($Au_{12}$−$Au_{14}$) and to three-dimensional (3D) hollow-cage ($Au_{16}$), pyramidal ($Au_{19}$), and core-shell structures ($Au_{27-28}$, $Au_{32-35}$, and $Au_{55}$) under the conventional bimolecular LH mechanism (Scheme 1a). A main result obtained in this study is that the core−shell clusters exhibit much higher activity toward CO oxidation than either 2D "flake"-like clusters or 3D "flat cage" structures. The surface protruded triangular $Au_3$


dx.doi.org/10.1021/ja309460v | J. Am. Chem. Soc. 2013, 135, 2583−2595

**Table 1. Comparison of Activation Energies ($E_a$ in eV) of CO Oxidation under Either Conventional Bimolecular LH or New Trimolecular Mechanism[a]**

| CO Oxidation under Bimolecular LH Mechanism (Involving One CO and One $O_2$ Molecule) | | | | | |
|---|---|---|---|---|---|
| | $E_a$(TS1) | $E_a$(TS2) | | $E_a$(TS1) | $E_a$(TS2) |
| $Au_8$ | 0.97 | 0.34 | $Au_7$ | 0.74 | 0.42 |
| $Au_{10}$ | 0.6 | 0.49 | $Au_9$ | 0.48 | 0.38 |
| $Au_{12}$ | 0.47−0.69 | 0.25−0.50 | $Au_{13}$ | 0.10−0.36 | 0.14−0.41 |
| $Au_{14}$ | 0.26−0.69 | 0.43−0.57 | $Au_{19}$ | 0.50 | 0.23−0.26 |
| $Au_{16}$ | 0.34 | 0.63−0.80 | $Au_{27}$ | 0.05−0.22 | 0.21−0.44 |
| $Au_{28}$ | 0.30−0.55 | 0.35−0.51 | $Au_{33}$ | 0.20−0.28 | 0.16−0.23 |
| $Au_{30}$ | 0.25−0.40 | 0.31−0.39 | $Au_{35}$ | 0.16−0.29 | 0.20−0.29 |
| $Au_{32}$ | 0.35−0.44 | 0.14−0.26 | $Au_{55}$ | 0.13−0.26 | 0.17−0.22 |
| $Au_{34}$ | 0.38−0.43 | 0.18−0.26 | | | |

| CO Oxidation under Trimolecular LH Mechanism (Involving *Two* CO Molecules and One $O_2$ Molecule) | | | | | | | |
|---|---|---|---|---|---|---|---|
| | $E_a$(TS1) | $E_a$(TS2)[b] | $E_a$(TS2)[c] | | $E_a$(TS1) | $E_a$(TS2)[b] | $E_a$(TS2)[c] |
| $Au_8$ | 0.9 | 0.3 | 0.41 | $Au_7$ | 0.44 | 0.64 | 0.46 |
| $Au_{10}$ | 0.58 | 0.55 | 0.38 | $Au_9$ | 0.59 | 0.09 | 0.23 |
| $Au_{12}$ | 0.5 | 0.3 | *d* | $Au_{13}$ | *d* | *d* | *d* |
| $Au_{14}$ | 0.38 | 0.18 | *d* | $Au_{19}$ | 0.09 | 0.05 | 0.32 |
| $Au_{16}$ | 0.29 | 0.1 | *d* | $Au_{27}$ | 0.10−0.28 | 0.01−0.12 | 0.41−0.65 |
| $Au_{28}$ | 0.15−0.61 | 0.11−0.27 | 0.42−0.59 | $Au_{33}$ | 0.17−0.32 | 0.02−0.13 | 0.40−0.54 |
| $Au_{30}$ | 0.20−0.55 | 0.06−0.16 | 0.32−0.67 | $Au_{35}$ | 0.17−0.29 | 0.05−0.15 | 0.38−0.57 |
| $Au_{32}$ | 0.27−0.41 | 0.02−0.16 | 0.45−0.47 | $Au_{55}$ | 0.19−0.32 | 0.01−0.05 | 0.47−0.49 |
| $Au_{34}$ | 0.41−0.54 | 0.04−0.19 | 0.48−0.55 | | | | |

[a]The definition of steps **TS1** and **TS2** is given in Figures 1−3. [b]The activation energy of O−O bond scission via the neighboring CO promoter. [c]The activation energy of O−O bond dissociation via the direct breaking of an O−O bond. [d]No corresponding transition state or reaction path is located. The corresponding energy data are available in Figures 1−3 and in Figures S1−S3 (Supporting Information). For $Au_{16}$ and $Au_{19}$, the energies are computed at the TPSSh/LANL2DZ (for Au) and 6-31G* (for C and O) levels. Other energies are computed at the PBE/DND level.

sites are identified as the most active sites of the gold clusters, which result in lower energy barriers for the CO oxidation. The second is the self-promoting CO oxidation mechanism. The triangular $Au_3$ active sites can not only stabilize the OCOO* intermediate and transition-state structure in the O−O scission step but also accommodate an additional CO molecule. As a result, the activation barrier for breaking an O−O bond is lowered from 0.2−0.5 eV (bimolecular LH mechanism, Scheme 1a) to 0.01−0.2 eV (the trimolecular mechanism, Scheme 1b). In addition, the CO self-promoting oxidation effect is also predicted to be viable on metal oxide supported gold clusters. However, the effect is less significant on the 2D planar or flat-cage gold clusters.

## 2. COMPUTATIONAL METHOD AND DETAILS

In this study, atomic structures of all nanosized gold clusters are taken from previously resolved global minimum structures on the basis of combined photoelectron spectroscopy (PES) measurements and density functional theory (DFT) global optimization.[73−77] The geometric structures of intermediates and transition states are optimized using either restricted or unrestricted DFT methods with the general gradient approximation (GGA) in the form of a Perdew−Burke−Ernzerhof (PBE) functional[78] or with the hybrid meta-GGA functional (TPSSh)[79] implemented in Dmol$^3$ 4.4[80] and Gaussian 09,[81] respectively. For the planar $Au_7$−$Au_{10}$, cage $Au_{16}$, and pyramidal $Au_{19}$ clusters, the TPSSh functional combined with the LAN2DZ basis set (for Au) and 6-31G* basis set for C and O are used for all energy computations. The energy reported here includes the zero-energy correction. For larger gold clusters, the PBE functional with a semicore pseudopotential (DSPP) is used, together with the double numerical (DND) basis set for the geometric optimization and transition-state search.

The reaction pathway for the CO oxidation is computed using a combination of linear synchronous transit (LST)/quadratic synchronous transit (QST) algorithms with conjugated gradient optimization. In the calculation of $O_2$ adsorption energy on Au clusters, and the first transition state to form the OCOO* intermediate, a fixed triplet spin is used for systems with an even number of total valence electrons, while a fixed doublet spin is used for systems with odd numbers of total valence electrons. For all other calculations, including intermediate states and final (product) states, the spin state of the system is set to be the singlet or doublet for systems with even or odd numbers of electrons. The unrestricted DFT is used for transition-state calculations. The convergence criteria of the geometrical optimization are set to be 1.0 × $10^{-5}$ hartree for the energy change, 2.0 × $10^{-3}$ hartree/Å for the gradient, and 3.0 × $10^{-3}$ Å for the displacement (in Dmol$^3$ computation), respectively. The smearing parameter is set to be 0.002 hartree in the geometric optimization. A zero smearing parameter is used for the density of states (DOS) analysis. Note that the spin crossover effect is not considered in this study, but the relative stabilities between triplet and singlet spin states of the intermediate and transition states are examined. Only the lowest energy states are reported.

## 3. RESULTS AND DISCUSSION

**3.1. Identification of Active Sites on Nanosized Gold Clusters.** To illustrate the effect of CO self-promoting oxidation, we first determined the most active site on the gold clusters. For the CO oxidation on metal oxide supported gold clusters, multiple active sites have been suggested, which include either sites on the gold cluster itself or perimeter sites near the Au and metal oxide interface. In the case of perimeter sites, a recent joint experimental/theoretical study shows that the CO molecule diffuses from the $TiO_2$ surface to the perimeter Au/$TiO_2$ site and then reacts with the $O_2$ molecule at the dual active site bridging Ti atom and gold nanowire.[26] A similar mechanism has also been suggested for Au clusters on MgO supports.[82,83] Here, our initial focus is placed on CO and $O_2$ adsorption on the gold clusters only. First, we examine single CO oxidation on various nanosized gold clusters (with sizes from 0.3 to 0.8 nm) under the conventional bimolecular LH mechanism (Scheme 1a). It is


dx.doi.org/10.1021/ja309460v | J. Am. Chem. Soc. 2013, 135, 2583−2595

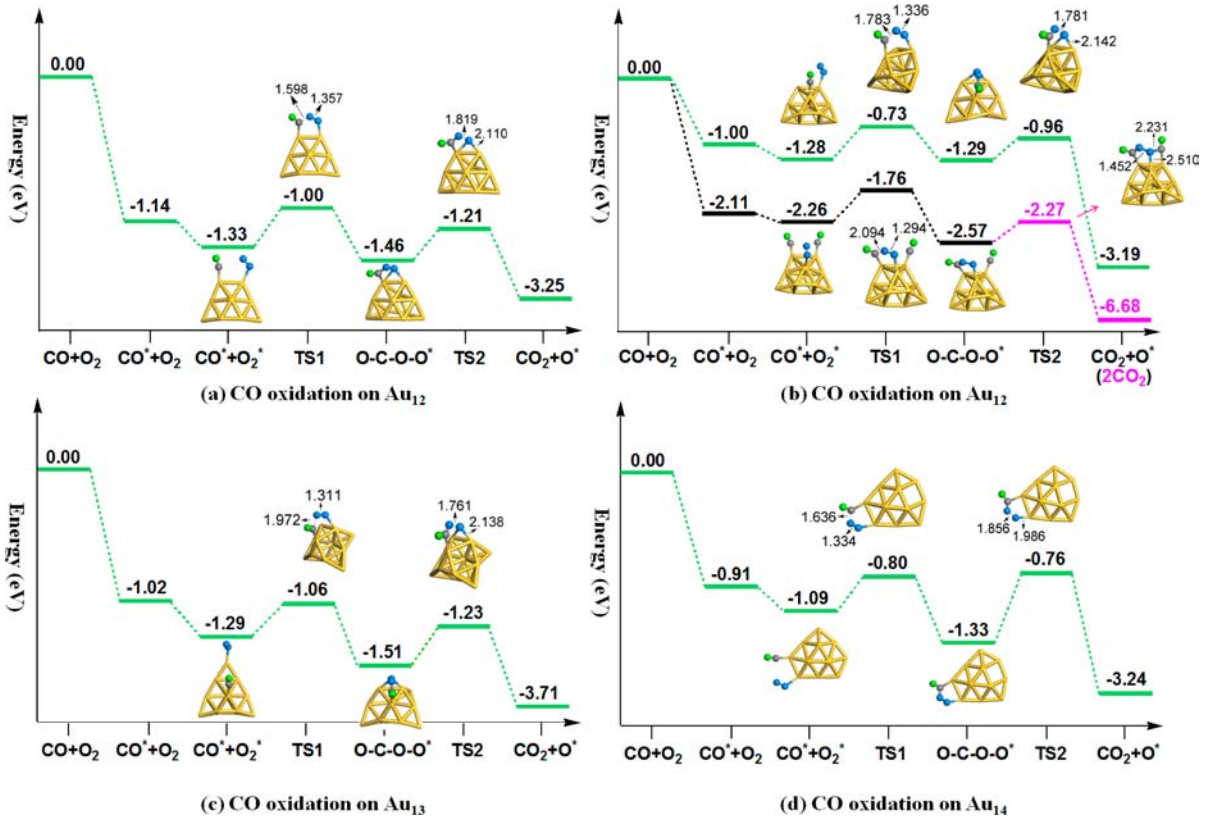


**Figure 1.** Energy diagrams of the most favorable pathways of CO oxidations on $Au_{12}$–$Au_{14}$ clusters (a–d). Various less favorable pathways at different sites are given in Figure S2 (Supporting Information). CO oxidation involving two CO molecules (black or pink path) is also shown in (b). The energies (in eV) are computed at the PBE/DND level. The bond length is in unit of Å. The absolute electronic energies and atomic coordinates of intermediates and transition states are given in the Supporting Information.

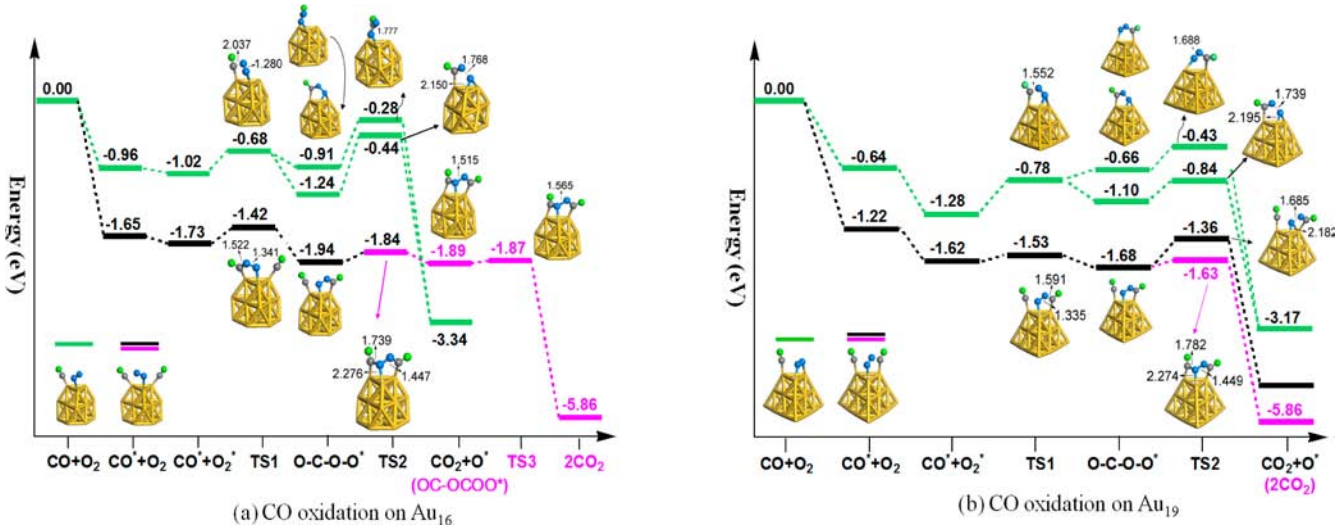


**Figure 2.** CO oxidation pathways on $Au_{16}$ and $Au_{19}$ clusters, involving either one (green path) or two CO molecules (black or pink path). The energy at each step is computed using the TPSSh functional with the LANL2DZ basis set for Au and 6-31G* basis set for C and O elements. Zero-point energy correction is included. The absolute electronic energies and atomic coordinates of intermediates and transition states are given in the Supporting Information.

known that strong relativistic effect of Au results in a late structural transition for anionic gold clusters from 2D to 3D at $Au_{12}$.[73−77] Here, we will consider planar clusters ($Au_7$–$Au_{10}$), flat- and hollow-cage clusters ($Au_{12}$–$Au_{14}$, and $Au_{16}$), the pyramid cluster $Au_{19}$, and core–shell clusters ($Au_{27–28}$, $Au_{30}$, $Au_{32–35}$, and $Au_{55}$).

*3.1.1. CO Oxidation on Planar and Flat-Cage Gold Clusters $Au_{7–10}$ and $Au_{12–14}$.* On the planar clusters, the CO oxidation reaction tends to occur on an edge site (active site), as shown in Figure S1 (Supporting Information). The barrier heights for two elemental reaction steps for the CO oxidation are summarized in Table 1, which are denoted as $E_a$(TS1) and $E_a$(TS2). On the


dx.doi.org/10.1021/ja309460v | J. Am. Chem. Soc. 2013, 135, 2583−2595

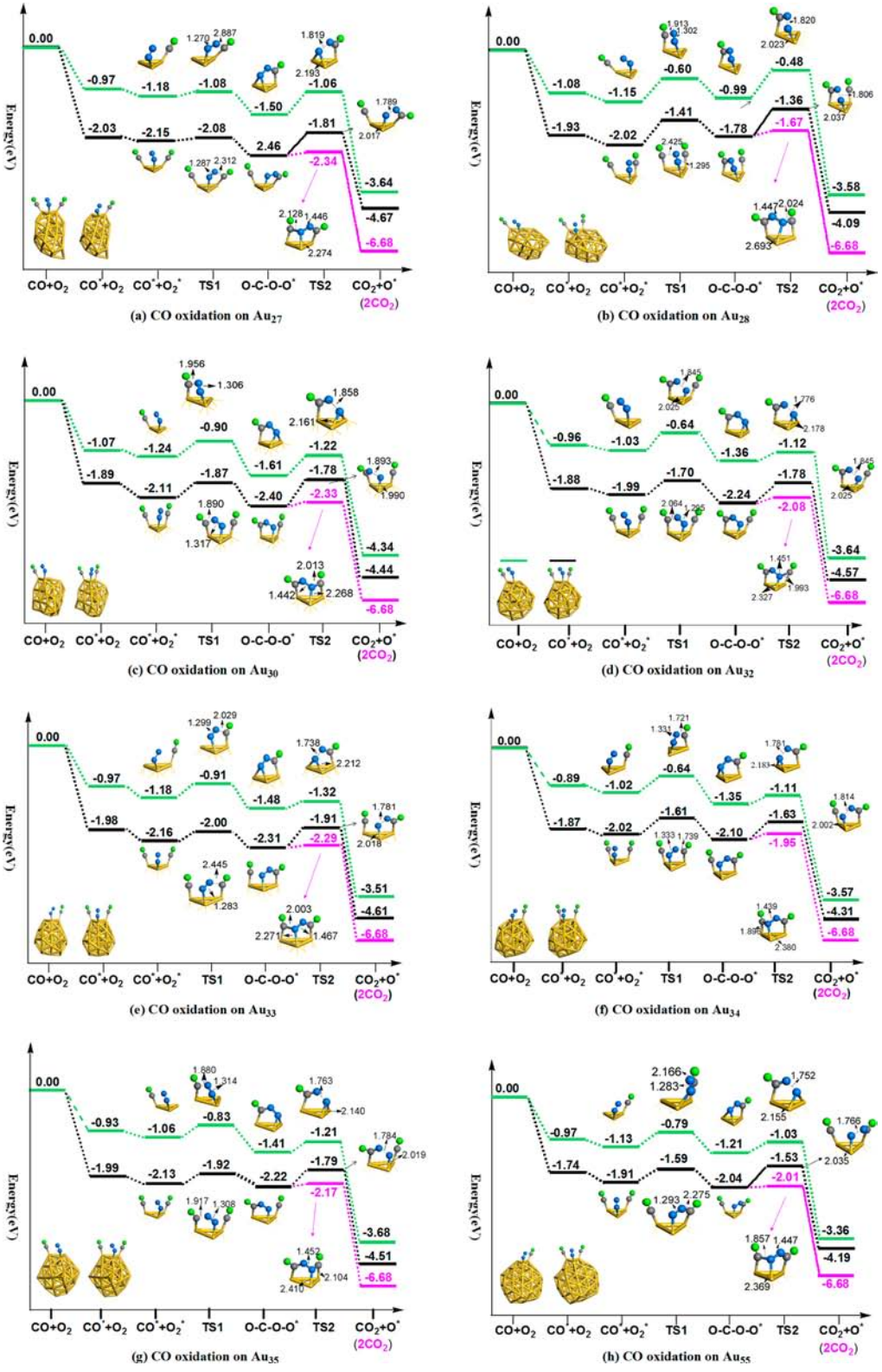


**Figure 3.** Most favorable pathways for CO oxidations on core−shell gold clusters (a) − (h). The reaction pathways at the same triangular $Au_3$ site but involving either single (green path) or double (black or pink path) CO molecules are compared. The energies are computed at the PBE/DND level. The absolute electronic energies and atomic coordinates of intermediates and transition states are given in the Supporting Information.

planar gold clusters, the formation of the OCOO* intermediate is the rate-determining step, with the energy barrier in the range of 0.48−0.97 eV, consistent with previous theoretical studies.[84]

With an increase in the Au cluster size, a 2D to 3D structural transition occurs.[76,85] The flat-cage clusters $Au_{12}$−$Au_{14}$ entail local structures more diverse than those of the planar clusters. For example, sharp edge sites and the protruded triangular $Au_3$ sites coexist on the surface. To identify the active sites for CO oxidation, we have examined various CO oxidation paths on different surface sites of $Au_{12}$−$Au_{14}$, as illustrated in Figure 1 (the


dx.doi.org/10.1021/ja309460v | J. Am. Chem. Soc. 2013, 135, 2583−2595

most favorable path) and Figure S2 (Supporting Information; other pathways). The energy barriers for two elemental reaction steps are summarized in Table 1. Among the flat-cage clusters $Au_{12}$–$Au_{14}$, $Au_{12}$ and $Au_{13}$ are predicted to exhibit relatively higher activity toward CO oxidation than $Au_{14}$ due to the lower energy barriers for both OCOO* formation (TS1) and the O–O bond-breaking step (TS2). In particular, we find that the CO oxidation can proceed on either the peripheral edge sites or the protruded triangular $Au_3$ sites. For even-numbered clusters ($Au_{12}$ and $Au_{14}$), the CO oxidation tends to occur on the sharp edge sites due to lower activation energy for both TS1 and TS2 in comparison to that on the triangular $Au_3$ site (Figure 1 and Figure S2). In contrast, for the odd-numbered cluster $Au_{13}$ the CO oxidation tends to occur on the protruded triangular $Au_3$ site, at which the highest energy barrier incurred is less than 0.36 eV.

*3.1.2. CO Oxidation on Hollow-Cage and Truncated-Pyramid Gold Clusters $Au_{16}$ and $Au_{19}$.* In the size range of $Au_{16}$ to $Au_{20}$, the gold clusters undergo structural transition from hollow cages to pyramids.[75] Beyond $Au_{20}$, the structure of gold cluster evolves into tubular-like and then core–shell structures.[76,77] Here, we select $Au_{16}$ and $Au_{19}$ as representative model clusters for the hollow-cage and vertex-truncated pyramid structures, respectively.

On the $Au_{16}$ cage, the CO oxidation tends to occur at the edge and the triangular $Au_3$ sites. In Figure 2a, we plot two pathways for the single CO oxidation at the edge site and triangle site, respectively. Again, the CO tends to be adsorbed on a less coordinated Au atom. The adsorption energy of a single CO molecule on $Au_{16}$ is −0.96 eV at a corner site of $Au_{16}$. The subsequent adsorption of an $O_2$ molecule at the neighboring Au corner site is slightly exothermic. With the coadsorption of CO and $O_2$ molecules, the nucleophilic attack of an $O_2$ molecule at the CO molecule leads to the formation of an OCOO* intermediate with an energy barrier of 0.34 eV. During this step, the OCOO* forms a single Au–O linkage at the edge site. However, the energy calculation indicates that the OCOO* intermediate formed at the edge site is less stable than the initially coadsorbed structure by 0.11 eV. Following this intermediate, the barrier for O–O scission at the edge site is 0.63 eV.

Figure 2a shows an alternative reaction path that involves the triangular $Au_3$ site. A more stable OCOO* intermediate structure may form through the conversion of the initially formed OCOO* intermediate at edge site to that on the triangular $Au_3$ site, where one O atom in the new OCOO* intermediate links with two Au atoms on the triangular $Au_3$ site. The formation of a double Au–O linked OCOO* intermediate at the triangular $Au_3$ site results in an additional stabilization of 0.33 eV in energy. The energy at the transition state can be notably lowered for the OCOO* intermediate at the triangular $Au_3$ site. On $Au_{19}$, a similar stabilization behavior for both the OCOO* intermediate and transition state structure is found at the triangular active site (see Figure 2b). It is expected that the CO oxidation may proceed more readily through the formation of an OCOO* intermediate on the triangular reaction site, which is designated as the most active site on $Au_{16}$ and $Au_{19}$.

*3.1.3. CO Oxidation on Core–shell Gold Clusters $Au_{27}$, $Au_{28}$, $Au_{30}$, $Au_{33-35}$, and $Au_{55}$.* Recent joint experimental/theoretical studies suggest that the core–shell structures are prevailing for gold clusters in the size range of 25–64 (up to 1.3 nm in diameter).[76,86] For example, the $Au_{27}$, $Au_{28}$, $Au_{30}$, $Au_{32-35}$, and $Au_{55}$ clusters can be viewed as having an inner Au core ($Au_1$–$Au_8$) and an outer shell. The shell typically consists of many slightly perturbed triangular $Au_3$ sites. As shown above, the perturbed triangular $Au_3$ site can effectively stabilize the OCOO* intermediate and the transition-state structure on $Au_{16}$ and $Au_{19}$ and become the most active site. Likewise, by examining the reaction pathway of single CO oxidation on different sites, we confirm that the triangular $Au_3$ sites are still the most active sites toward CO oxidation, as illustrated in Figure 3 and Figure S3 (Supporting Information). Typically, the adsorption energy of an initial CO molecule on the core–shell clusters ranges from −0.7 to −1.2 eV, comparable to those on the planar and flat-cage clusters. Subsequent coadsorption of an $O_2$ molecule at the same triangular $Au_3$ site is slightly exothermic, with the $O_2$ adsorption energy ranging from −0.05 to −0.3 eV (Figure 3 and Figure S3 (Supporting Information)), close to the measured value (about −0.088 eV at 280 K).[87]

*3.1.4. "Odd–Even" Effect.* Table 1 summarizes computed activation energies associated with two elemental reaction steps at different reaction sites of the core–shell clusters. An interesting "odd–even" behavior for the activation energies with respective to the number of gold atoms can be observed in the formation of the OCOO* intermediate ($E_a$(TS1)). The CO oxidation on gold clusters with odd-numbered atoms ($Au_{13}$, $Au_{27}$, $Au_{33}$, $Au_{35}$, $Au_{55}$) generally encounters an activation barrier to the formation of OCOO* intermediate lower than that on even-numbered gold clusters ($Au_{12}$, $Au_{14}$, $Au_{28}$, $Au_{30}$, $Au_{32}$, $Au_{34}$). Such an *odd–even* effect is more pronounced with the core–shell clusters, as shown in Table 1. The origin of such an odd–even effect may be attributed to different extents of activation of the $O_2$ molecule on the odd- and even-numbered clusters. The $O_2$ binding and activation have been considered as key steps during CO oxidation. Although numerous experimental and theoretical studies have shown that the $O_2$ molecule cannot dissociate on the gold clusters,[88−90] the odd–even effect is already known such that gold clusters with odd numbers of electrons can bind with the $O_2$ molecule more strongly, thereby leading to a higher degree of activation of the $O_2$ molecule. For gold cluster anions with even numbers of electrons, some electrons can be transferred to the unoccupied $2\pi^*$ orbital to active the $O_2$ molecule.[91] In particular, a superoxo to peroxo transition for $O_2$ adsorbed on $Au_8^-$ has been detected in a recent study.[92] In the present study, a partial density of state (PDOS) analysis indicates that the $O_2$ molecule adsorbed on an even-numbered gold cluster preserves the triplet spin state, as in the gas phase. Considering the spin-conservation paradigm during the chemical reaction, we expect a spin-flipping process that may occur during the formation of the OCOO* intermediate on an even-numbered gold cluster. However, a direct calculation of such a process is rather complicated. Here, a single-reference DFT method is utilized to describe TS1 at a different but fixed spin state (e.g., singlet or triplet state).

*3.1.5. Key Role of Triangular $Au_3$ Active Site.* The key role of the triangular $Au_3$ active site can be understood from its stabilization effect on the structure of the OCOO* intermediate and the O–O bond-breaking transition state. In Figure 4, we illustrate energies of the OCOO* intermediate and the following O–O bond-breaking state at the edge site and at the triangular $Au_3$ site, respectively, on $Au_{16}$, $Au_{19}$, and various core–shell gold clusters. The stabilization effect of the triangular $Au_3$ site over the edge site can be clearly seen in that the OCOO* intermediate is more stabilized by increasing the number of Au–O linkages on a triangular active site. The gained stabilization energy ranges from −0.05 to −0.30 eV on the triangular active site. The energy barrier for the interconversion between the two different intermediate structures is computed at various active sites on

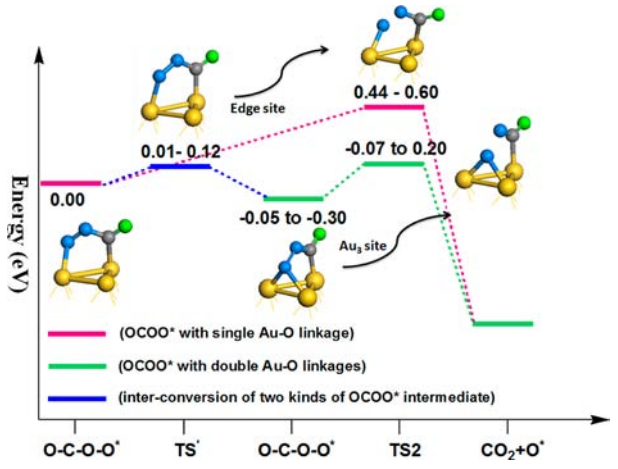


**Figure 4.** Comparison of reaction pathways of CO oxidation (involving only single CO) at the edge site (pink path) and triangular $Au_3$ active site (blue-green path). The energies are computed at the PBE/DND level.

different core−shell gold clusters (Figure S4, Supporting Information). The energy barrier for the structural transition from the intermediate with a single Au−O linkage to that with double Au−O linkages is quite small (<0.12 eV), indicating possible fast conversion of the OCOO* intermediate from single to double Au−O linkages. A comparison of the energy barrier of the next O−O bond-breaking step starting from the two different intermediate structures suggests that the activation energy of O−O dissociation decreases significantly (nearly 50% percent) when the formation of a transition state structure involves double Au−O linkages, as shown in Figure 4.

The finding of triangular $Au_3$ sites as the most active sites allows us to determine which factor plays a more important role in the CO oxidation: for example, electronic effects versus the local geometric structure. It was previously shown that unsupported porous bulk gold is active in CO oxidation, suggesting that the microsurface nanostructure is crucial to the catalytic activity.[31,32a] Here, our studies suggest that several gold clusters, such as $Au_{32}$, $Au_{33}$, $Au_{35}$, and $Au_{55}$, have comparable or even slightly higher activities than the magic-numbered cluster $Au_{34}$ (see Figure 3 and Table 1). The similarity in activities for these clusters with different numbers of valence electrons can be attributed to the universal presence of triangular $Au_3$ active sites, which not only can favorably adsorb CO and $O_2$ molecules but also offer additional stabilization to both the reaction intermediate (OCOO*) and the transition-state structure during O−O scission. More information regarding this view of active sites is given in Figure S5 (Supporting Information), which shows a systematic study of CO oxidation on a series of model vertex-truncated tetrahedral gold clusters, ranging from $Au_{34}$ to $Au_{147}$ (diameter ranges from 0.4 to 1.9 nm). All of these calculations indicate that the O−O scission barrier at the triangular $Au_3$ active site is insensitive to the cluster size.

**3.2. CO Self-Promoting Oxidation at the Triangular $Au_3$ Active Site.** Having shown that the perturbed triangular $Au_3$ sites are the most active sites on nanosized 3D gold clusters for the CO oxidation, we demonstrate that multiply adsorbed CO molecules at a triangular $Au_3$ active site can significantly promote the CO oxidation as well. As mentioned above, it is known that coadsorbed water molecule can promote CO or propene oxidation through activation of an $O_2$ molecule.[93] Likewise, recent studies show that a coadsorbed CO molecule can also significantly promote alcohol electrochemical oxidation and its own electrochemical oxidation on gold surfaces.[71,72] Nonetheless, few studies take into account the role of coadsorbed CO molecules when discussing the CO oxidation mechanism. In the case of CO oxidation on gold clusters with or without supports, several experimental measurements have indicated the possibility of coadsorption of multiple CO molecules at or near active sites,[64−69] which is also visualized from the molecular dynamics simulations.[70]

Here, we consider two CO molecules occupying two corners of a triangular $Au_3$ active site while an $O_2$ molecule is adsorbed on a neighboring corner as shown in Figures1b, 2, and 3. The energy diagrams in Figures 1−3 give the coadsorption energies of the two neighboring CO molecules, which demonstrate that the coadsorption of two CO molecules at the triangular active site is energetically favorable. Due to the adsorption of multiple molecules on the same triangular $Au_3$ site, the triangular $Au_3$ site becomes more protruded. Here, we define an out-of-plane angle to characterize the degree of protrusion for a triangular $Au_3$ site (see Figure S6, Supporting Information). The calculated out-of-plane angles on various core−shell gold clusters indicate that the coadsorption of an additional CO molecule generally increases the cone angle of the local Au site, thereby increasing the out-of-plane angle at the same $Au_3$ site. The increased out-of-plane angle not only slightly enhances the $O_2$ adsorption in general (see Figures 1−3) but also results in a shorter distance between the $C_{CO}$ atom and neighboring O atom in the OCOO* unit. For example, a triangular $Au_3$ site on $Au_{19}$ gives rise to the largest out-of-plane angle (62°) among all triangular $Au_3$ sites examined on 3-D gold clusters larger than $Au_{16}$, which results in the shortest $C_{CO}\cdots O_{OCOO*}$ distance (~2.40 Å). Moreover, the increased out-of-plane angle also inhibits the conversion of OCOO* intermediate due to the increased Au−O linkage, even though this step is energetically favorable under the conventional bimolecular LH mechanism.

As shown in Table 1, a major effect due to the coadsorbed neighboring CO molecule on the CO oxidation is that the O−O dissociation energy barrier ($E_a$(TS2)) is notably reduced, in comparison to that in the single CO oxidation path or that in the direct breaking of a O−O bond without the promotion by the additional CO. We call such an effect *CO self-promoting oxidation* or CO-induced O−O activation. As an example, the $Au_{16}$ cluster is a less efficient catalyst in comparison to other clusters due to the high activation energy required in the O−O scission step under the bimolecular LH mechanism. In contrast, Figure 2 shows that the neighboring CO molecule can markedly promote O−O bond breaking under the trimolecular mechanism. Under the latter mechanism, the first step is the same as that under the conventional bimolecular LH mechanism in that the $O_2$ molecule attacks nucleophilically a neighboring CO molecule to form the OCOO* intermediate. In this step, the additional neighboring CO molecule has little effect on the energy barrier. The second reaction step can proceed in two possible ways: direct O−O bond scission from the OCOO* intermediate or the electrophilic attack of the OCOO* intermediate by the additional CO molecule. In the latter way, the energy barrier is as low as 0.10 eV, resulting in the formation of a metastable OC−OCOO* intermediate, as shown in Figure 2a. The O−O bond is elongated to 1.52 Å in this intermediate. The OC−OCOO* intermediate can readily proceed to the breaking of the O−O bond after crossing a very low energy barrier (0.02 eV), leading to the spontaneous formation of two $CO_2$ molecules at a time. An intrinsic reaction coordinate (IRC) analysis was performed to confirm the formation of the metastable intermediate (Figure S7,


dx.doi.org/10.1021/ja309460v | J. Am. Chem. Soc. 2013, 135, 2583−2595

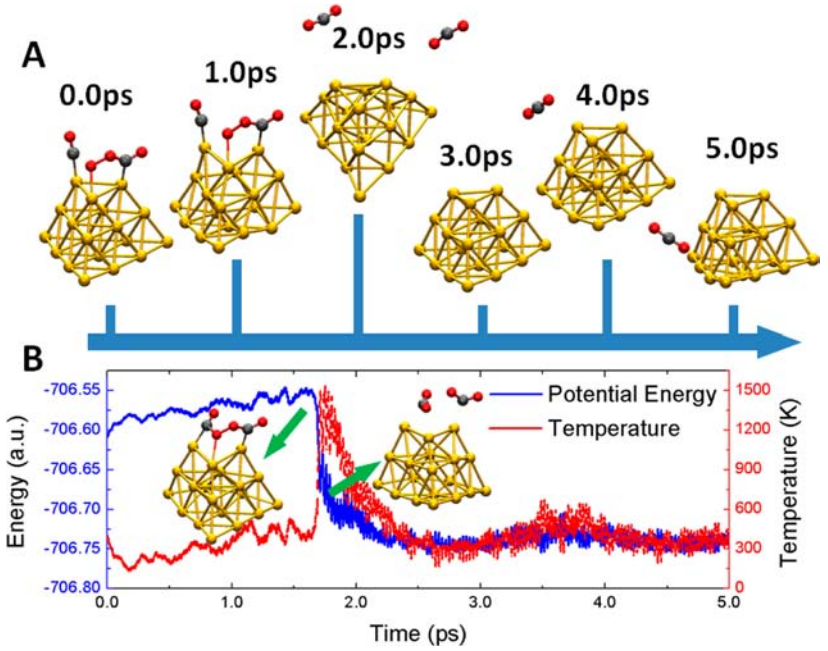


**Figure 5.** Born−Oppenheimer molecular dynamics (BOMD) trajectory of the CO self-promoting oxidation process: (A) snapshots of intermediate at different simulation times; (B) computed potential energy and temperature in the course of the BOMD simulation.

Supporting Information). As another example, a similar reaction path is seen in the case of pyramidal $Au_{19}$. However, we find that the activation energy of the first OCOO* formation step is lowered significantly from 0.39 to 0.09 eV when two CO molecules are coadsorbed on a triangular $Au_3$ site of $Au_{19}$. In the second O−O bond-breaking step, the activation energy of O−O scission due to the electrophilic attack of the additional CO molecule at the OCOO* intermediate is as low as 0.06 eV, significantly lower than that (0.33 eV) through a direct dissociation of the O−O bond from the OCOO* intermediate. Here, the electrophilic attack from the additional CO molecule at the OCOO* intermediate on $Au_{19}$ leads to two $CO_2$ molecules to complete the catalytic cycle, without the formation of a metastable OC−OCOO* intermediate. Indeed, for all other core−shell gold clusters ($Au_{27}$, $Au_{28}$, $Au_{30}$, $Au_{32}$−$Au_{35}$, and $Au_{55}$) considered, the additional CO also promotes O−O scission at the triangular $Au_3$ site, as shown in Figure 3 and Table 1. In particular, we find that such a CO-induced O−O scission effect is more pronounced on some more spherical-like gold clusters such as $Au_{32}$−$Au_{35}$ and $Au_{55}$. The O−O bond-breaking barrier, caused by the attack of the additional CO molecule, is typically less than 0.1 eV, which is much lower than that from direct O−O dissociation. The much favored CO-induced O−O bond scission on $Au_{16}$, $Au_{19}$, $Au_{32}$−$Au_{35}$, and $Au_{55}$ in comparison to that on other clusters such as $Au_{27}$ and $Au_{28}$ can be attributed to the smoother surface curvature, where the triangular $Au_3$ sites exhibit out-of-plane angles ranging from 33 to 62°.

Note that such a CO self-promoting effect is less pronounced on 2D planar gold clusters ($Au_7$−$Au_{10}$) and flat-cage clusters ($Au_{12}$−$Au_{14}$). The CO-promoted O−O dissociation barriers for these clusters are comparable to or even slightly higher than those via the direct scission of an O−O bond from the OCOO* intermediate under the bimolecular CO oxidation mechanism (see Figure 1b and Figures S1 and S2 (Supporting Information)). The lack of a CO self-promoting effect is understood from a different structure around the active site. On planar gold clusters, the transition state structure from the OC···OCOO* intermediate exhibits a dangling conformation at the edge of the cluster, as shown in Figure S1. In contrast, OC···OCOO* is well stabilized by the triangular $Au_3$ site on $Au_{16}$, $Au_{19}$, and other core−shell gold clusters, evidenced by the short distance between the middle O atom in the OC···OCOO* intermediate and surface Au site, hence leading to a reduced energy barrier. For flat-cage gold clusters, the triangular $Au_3$ sites typically exhibit quite large out-of-plane angles (>90°), which result in a relatively long distance between $C_{CO}$ and $O_{OCOO*}$ atoms and hence a higher energy barrier during the electrophilic attack of $C_{CO}$ at OCOO*.

In several previous theoretical studies, the formation of the initial OCOO* intermediate has been viewed as the rate-determining step for CO oxidation due to the relatively higher energy barrier encountered in this step.[94,95] However, little experimental evidence is available to confirm this view. The present study indicates that the energy barrier to the formation of the OCOO* intermediate on even-numbered gold cluster is generally much higher than that on odd-numbered gold clusters such as $Au_{27}$, $Au_{33}$, and $Au_{55}$. For odd-numbered clusters, the O−O dissociation step generally entails an energy barrier higher than or comparable to that of the first step (cf. Table 1). In the present study, we have shown that the coadsorbed neighboring CO molecule can notably lower the energy barrier of O−O scission, which may lead to a high turnover frequency for CO oxidation.

**3.3. Evidence of CO Self-Promoting Oxidation from Born−Oppenheimer Molecular Dynamics (BOMD) Simulation.** For all gold clusters considered, $Au_{19}$ appears to possess the highest catalytic activity with the assistance of CO self-promotion. The CO oxidation is nearly barrierless, with the highest energy barrier to the OCOO* formation being only 0.09 eV. Thus, it is conceivable to observe the O−O scission directly in molecular dynamics simulations under thermal fluctuations. Here, three independent BOMD trajectories (each lasts 5 ps) are attained, all starting from the optimized CO*···OCOO* intermediate. The BOMD simulations are performed based on a DFT method with a mixed Gaussian and plane-wave (GPW)


dx.doi.org/10.1021/ja309460v | J. Am. Chem. Soc. 2013, 135, 2583−2595

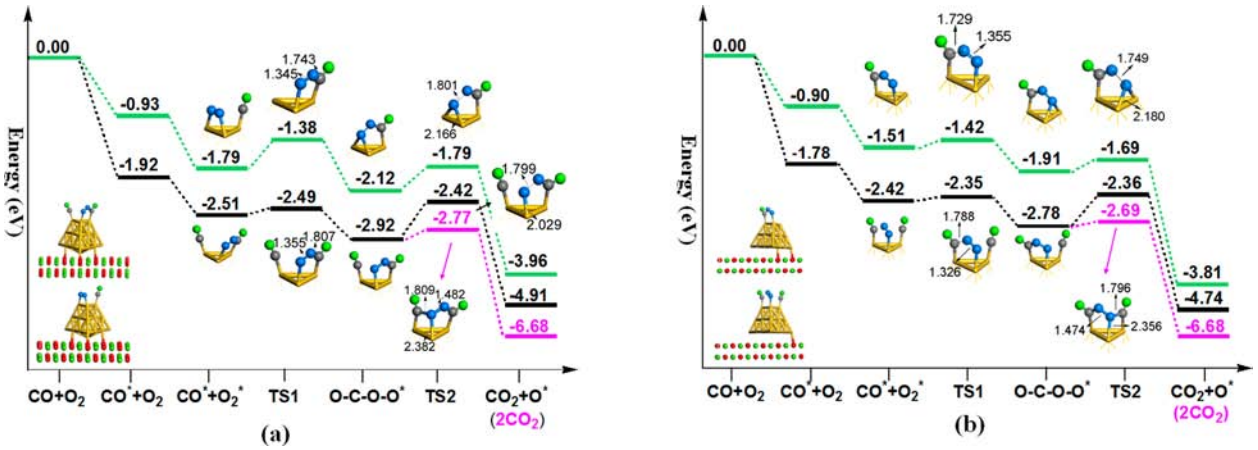


**Figure 6.** Bimolecular LH and CO self-promoted oxidation of CO oxidation on (a) F-center MgO and (b) vacancy free MgO supported $Au_{19}$. The energies are computed at the PBE/DND level.

basis.[96] The PBE functional with the DZP-MOLOPT[97] basis set is used to compute the exchange-correlation energy; the energy cutoff is set to be 80 Ry for the plane-wave wave functions. The interaction between the valence electrons and the atomic cores is accounted for using the Goedecker−Teter−Hutter (GTH) pseudopotential[97,98] as implemented in the CP2K code.[99] The constant-energy and constant-volume ensemble is adopted in all simulations.

Indeed, one BOMD trajectory (see the movie in the Supporting Information) demonstrates the CO-promoted O−O scission process within 5 ps simulation time. The spontaneous formation of two $CO_2$ molecules upon the approach of the $O_{OCOO}$ atom to the CO molecule is observed (see Figure 5). A more detailed analysis of the potential energy shows an abrupt drop in the potential energy in the time interval of 1.65−1.75 ps, accompanied by a dramatic increase of the system temperature. In this time interval, one can observe that the additional CO molecule approaches closely to the OCOO* species, leading to rapid O−O bond breaking to form two $CO_2$ molecules as final products, consistent with the transition-state picture obtained from the transition state search (Figure 2b). At the end of the reaction, the temperature of the system decreases rapidly to about 300 K, and the original structure of $Au_{19}$ was well retained.

In two other trajectories starting with different initial velocities, no O−O bond-breaking event is observed within 5 ps simulation. Although the same initial structure and temperature are used in the three independent simulations, different trajectories result due to the random atomic motion. By examining the OCOO* intermediate and transition-state structure of CO-promoted O−O dissociation, we find that the interatomic distance between $O_{OCOO}$ and $C_{CO}$ in the transition state is much shorter (by 0.7 Å) than that in the OCOO* intermediate. Hence, an elongated simulation time is needed in the other two simulations to allow the close encounter of $O_{OCOO}$ with $C_{CO}$ to occur.

**3.4. CO Self-Oxidation on Metal Oxide Supported Au Nanostructures and Microkinetic Analysis.** We have shown that the protruded triangular $Au_3$ sites on bare nanosized gold clusters are highly active sites for CO oxidation. An important question remains as to whether the CO self-promoting oxidation mechanism is generic: for example, is also viable on supported gold clusters or nanostructures. In view of the fact that the metal oxide support is widely used in heterogeneous gold catalysis to enhance catalytic activities, we also independently examined two metal oxide supported Au systems: (1) $Au_{19}$ on MgO (with or without oxygen vacancy) and (2) bilayer Au nanostructure on the (110) surface of rutile $TiO_2$. For the latter, previous experiments have shown that the bilayer gold nanostructures exhibit much higher activity than monolayer or trilayer gold nanostructures.[19] It is thus important to cross-examine the trimolecular LH mechanism with the bilayer gold nanostructures, which possess abundant triangular sites on the edge faces.

A variety of reaction pathways on different triangular $Au_3$ active sites of $Au_{19}$/MgO and bilayer Au/$TiO_2$ are attained, from which we find that the additional CO molecule can also promote O−O bond breaking via the trimolecular mechanism, regardless of the local structure of the underlying support. The energy barriers for the CO-promoted O−O bond breaking are 0.09 and 0.15 eV, respectively, on MgO and F-centered MgO supported $Au_{19}$; both are notably lower than those (0.22 and 0.33 eV) under the conventional bimolecular LH mechanism (see Figure 6). A similar promoting effect is observed with the bilayer Au/$TiO_2$ system, in which the corresponding energy barriers of O−O bond breaking are as low as 0.09 and 0.18 eV, respectively, much lower than that associated with the single-molecule reaction (0.37 eV; shown in Figure 7). This conclusion is consistent with that for the bare gold clusters.

To further compare the difference between bi- and trimolecular mechanisms, we have undertaken detailed microkinetic analysis for the reaction associated with both bare and supported gold clusters. The details of microkinetic analysis are given in the Supporting Information as part II. The microkinetic analysis suggests that the reaction rate of CO oxidation on the metal oxide supported gold clusters under the trimolecular mechanism is several times higher than that under the bimolecular process (see Table 2), which again confirms the promoting effect of coadsorbed neighboring CO molecules on the CO oxidation. Note, however, that the order of the reaction rate under the bimolecular and trimolecular mechanisms is mixed on the bare gold clusters (see Table S1, Supporting Information). Some bare gold clusters such as $Au_{16}$, $Au_{19}$, $Au_{30}$, and $Au_{33}$ favor the trimolecular mechanism over the bimolecular mechanism owing to the much higher reaction rate. Note also that the absolute value of the calculated reaction rate is strongly dependent on the $O_2$ adsorption energy. Here, the relatively high reaction rate of CO oxidation on $Au_{19}$/MgO is largely due to the strong $O_2$ adsorption.

**3.5. Origin of the CO Self-Promoting Oxidation.** Finally, to understand why the coadsorbed neighboring CO molecule


dx.doi.org/10.1021/ja309460v | J. Am. Chem. Soc. 2013, 135, 2583−2595

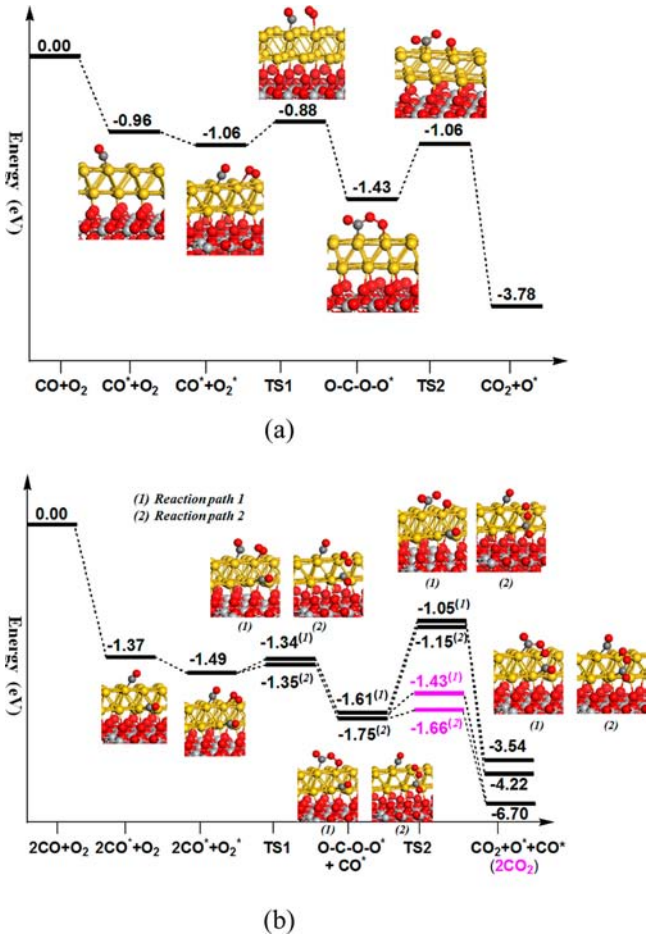


**Figure 7.** Comparison of energy diagrams of (a) bimolecular LH and (b) CO self-promoting oxidation on bilayer Au/$TiO_2$. In (b), two different reaction pathways are presented. In reaction path 1, $O_2$ first attacks the upper adsorbed CO molecule to form an OCOO* intermediate, and then either the O−O bond breaks directly or the breaking is induced by the attack of the neighboring CO molecule (in pink). In reaction path 2, the $O_2$ first attacks the lower adsorbed CO molecule to form an OCOO* intermediate, and then either the O−O bond breaks directly or the breaking is induced by the attack of the neighboring CO molecule. The energies are computed at the PBE/DND level. The model system includes a three-layer slab of $TiO_2$ and 24 Au atoms. The lengths of the supercell in the *x* and *y* directions (parallel to the slab) are 11.84 and 19.49 Å, respectively, and the length of the vacuum region in the *z* direction (normal to the slab) is 15 Å.

**Table 2. Calculated Reaction Rates of the CO Oxidation via Bimolecular and Trimolecular Mechanisms for Metal-Oxide Supported Gold Nanostructures**[a]

| | reaction rate ($s^{-1}$) | |
|---|---|---|
| Au system | bimolecular mechanism | trimolecular mechanism |
| $Au_{19}$/MgO with F center | $1.71 \times 10^5$ | $8.19 \times 10^5$ |
| $Au_{19}$/MgO | $4.48 \times 10^7$ | $1.59 \times 10^8$ |
| bilayer Au/$TiO_2$ | $3.30 \times 10^{-4}$ | $2.31 \times 10^{-3}$ (path 1)<br>$3.42 \times 10^{-3}$ (path 2) |

[a]Note that the $O_2$ adsorption energy can significantly affect the value of reaction rate: that is, because of stronger $O_2$ adsorption, the $Au_{19}$/MgO system yields a much higher reaction rate than the bilayer−Au/$TiO_2$ system. Details of microkinetic analysis are given in the Supporting Information.

can significantly promote the O−O scission, we display computed Hirshfeld atomic charges of $C_{co}$ and $O_{ocoo*}$ (in the coadsorbed neighboring CO molecule and OCOO* unit) for the OC*···OCOO* intermediate and at the transition state on $Au_{16}$ and $Au_{19}$ clusters, respectively (see Figure 8a,b). It is found that

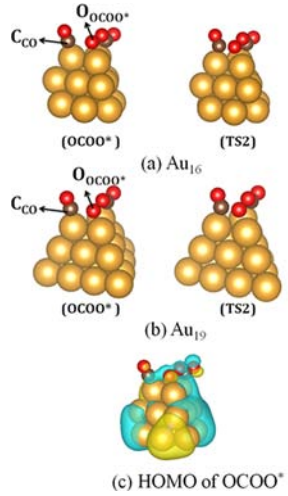


Hirshfeld atomic charge (|e|)

| | OCOO* | TS2 |
|---|---|---|
| $C_{CO}$ | 0.12 | 0.08 |
| $O_{OCOO*}$ | -0.21 | -0.12 |

**Figure 8.** Change of atomic charge from the OCOO* intermediate to the O−O scission transition state, upon the approach of $C_{CO}$ to $O_{OCOO*}$ on (a) $Au_{16}$ and (b) $Au_{19}$ clusters. (c) Electron density contour of the HOMO of the OCOO* intermediate on $Au_{16}$. The Hirshfeld charge analysis is based on calculations at the PBE/DND level.

the C atom is positively charged and O atom is negatively charged in both the intermediate and transition-state structures. However, when the $C_{co}$ and $O_{ocoo*}$ atoms approach to each other and reach the transition state, a charge transfer is observed between the two atoms: that is, the $C_{co}$ atom becomes less positively charged and the atomic charge on $O_{ocoo*}$ becomes less negative, as shown in Figure 8. The change in the charge on $C_{co}$ and $O_{ocoo*}$ atoms plays a key role in the CO-promoted activation of the O−O bond, which is an indicator of the electrophilic attack of the neighboring $C_{co}$ at the OCOO* unit. Moreover, the computed electronic density corresponding to the HOMO of the OCOO* intermediate with the presence of a coadsorbed neighboring CO molecule (Figure 8c) exhibits an overlap of the molecular orbitals of $C_{co}$ and $O_{ocoo*}$ due to the short interatomic distance. Hence, we conclude that the polar nature of a coadsorbed neighboring CO molecule (with the C atom being positively charged) on the perturbed $Au_3$ active site (which causes a shorter distance between CO and the OCOO* intermediate) contributes altogether to the CO self-promoting oxidation. On the other hand, due to the electrophilic attack of the CO molecule at the OCOO* species, the O−O bond length in the OCOO* species is slightly elongated. From Figures 2 and 3 and Figures S2 and S3 (Supporting Information), the O−O bond length in the CO-induced O−O activation transition state (TS2) is in generally less than 1.47 Å, which is much shorter than that involved in the transition state of direct O−O bond breaking (generally larger than 1.70 Å). We conclude that the electrophilic attack of the neighboring CO molecule accelerates the O−O activation and bond breaking through thermal fluctuation, as observed in the BOMD simulation (Figure 5).

To further confirm the generic role of the additional CO molecule in promoting the O−O scission, we have carried out a separate study of CO- and styrene-promoted styrene oxidation, as shown in Figure 9. Several previous studies have shown that


dx.doi.org/10.1021/ja309460v | J. Am. Chem. Soc. 2013, 135, 2583−2595

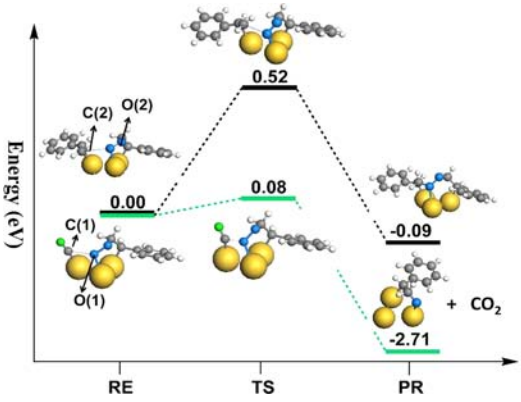


| | RE | TS |
|---|---|---|
| C(1) (\|e\|) | 0.11 | 0.08 |
| O(1) (\|e\|) | -0.20 | -0.14 |
| d(C(1)-O(1)) | 2.660 Å | 1.894 Å |
| C(2) (\|e\|) | -0.09 | -0.04 |
| O(2) (\|e\|) | -0.20 | -0.17 |
| d(C(2)-O(2)) | 3.044 Å | 2.065Å |

**Figure 9.** (left) Computed reaction pathways that illustrate the role of the coadsorbed neighboring CO or styrene molecule in the trimolecular O−O scission step during the styrene oxidation. (right) Hirshfeld atomic charges and atomic distances of C and O atoms involved in the electrophilic reactions. The energies are computed on the basis of the TPSSh functional with the LANL2DZ basis set for Au and 6-31G* basis set for C and O elements (zero-point energy correction is the included in the energy values). The same level of theory is used to evaluate the Hirshfeld atomic charges.

the styrene oxidation on gold catalysts entails a mechanism similar to that for the CO oxidation, such that the styrene molecule first forms a CCOO* intermediate, followed by O−O bond breaking to yield the product.[20,100−102] Here, we find that the coadsorbed neighboring styrene is not as efficient as CO in promoting the O−O scission, as the corresponding energy barrier is 0.52 eV, close to that reported previously under the conventional bimolecular mechanism.[102] However, we find that if the coadsorbed neighboring styrene molecule is replaced by a CO molecule, the styrene oxidation exhibits a very low barrier of 0.08 eV, suggesting a significant CO promotion effect toward the O−O bond breaking. After examination of the atomic charges of reactant and transition state structures, we find a major difference is that the terminal C atom in the coadsorbed neighboring styrene molecule is negatively charged in the course of the reaction, which would increase the electrostatic repulsion between C and O atoms in the transition state and hence the energy barrier. This independent study confirms again that the polar nature of the CO molecule plays a key role in promoting O−O bond scission under the trimolecular mechanism.

## 4. CONCLUSIONS

Our comprehensive DFT studies of CO oxidations on bare and metal oxide supported gold clusters suggest that the protruded triangular $Au_3$ site is the main active site on nanosized gold clusters. The triangular active site can stabilize both the reaction intermediate (OCOO*) and O−O bond-breaking transition state in the framework of the classic bimolecular LH mechanism. On the basis of the uncovered triangular active site, we find that the coadsorbed CO molecule at the active site can serve as a promoter for the scission of the O−O bond during CO oxidation, which can lead to spontaneous formation of two $CO_2$ molecules in one step. The energy barrier of O−O scission caused by the attack of coadsorbed neighboring CO molecule is much lower than that for the direct breaking of a O−O bond in the conventional bimolecular LH process. Our studies also indicate that such a CO self-promoting oxidation effect is rather generic, associated not only with bare gold clusters but also with the metal oxide supported gold clusters such as in the $Au_n$/MgO and bilayer Au/$TiO_2$ systems. The underlying mechanism for the CO self-promoting oxidation effect can be attributed to the polar nature of coadsorbed neighboring CO and the protruded $Au_3$ active site.

## ■ ASSOCIATED CONTENT

### Supporting Information

Text, figures, and tables giving computed CO oxidation pathways on different sites of gold clusters, a comparison of the O−O bond dissociation barrier of OCOO* intermediates at the edge and triangular sites on different core−shell gold clusters, activation energies of O−O scission versus the size and layer of pyramid gold clusters, an IRC analysis of CO-induced O−O scission on $Au_{16}$, the definition of the out-of-plane angle of a triangular $Au_3$ site (Figures S1−S7), a video displaying the CO oxidation process via the trimolecular mechanism, details of the micro-kinetic analysis, the complete ref 81, and the coordinates and absolute electronic energies of intermediates and transition states. This material is available free of charge via the Internet at http://pubs.acs.org.

## ■ AUTHOR INFORMATION

### Corresponding Author

E-mail: ypnku78@gmail.com (Y.P.); xzeng1@unl.edu (X.C.Z.).

### Notes

The authors declare no competing financial interest.

## ■ ACKNOWLEDGMENTS

Y.P. is supported by the Natural Science Foundation of China (Grant No. 21103144) and Hunan Provincial Natural Science Foundation of China (12JJ7002, 12JJ1003). X.C.Z. is supported by grants from the NSF (EPS-1010674) and ARL (W911NF1020099), a grant from USTC for (1000plan) Qianren-B summer research, and by the University of Nebraska's Holland Computing Center and the Center for Functional Nanomaterials (CFN) Theory and Computation Facility in Brookhaven National Laboratory (Research carried out in part at the Center for Functional Nanomaterials, Brookhaven National Laboratory, which is supported by the U.S. Department of Energy, Office of Basic Energy Sciences, under Contract No. DE-AC02-98CH10886). X.W. is supported by the National Basic Research Program of China (Nos. 2011CB921400, 2012CB922001), NSFC (grant no. 21121003, 11004180, 51172223), and the one Hundred Person Project of CAS.

## REFERENCES


(1) (a) Haruta, M.; Kobayashi, T.; Samo, H.; Yamada, N. *Chem. Lett.* **1987**, *2*, 405−408. (b) Haruta, M.; Yamada, N.; Kobayashi, T.; Iijima, S. *J. Catal.* **1989**, *115*, 301−309.
(2) Bailie, J. E.; Hutchings, G. J. *Chem. Commun.* **1999**, 2152−2152.
(3) Landon, P.; Collier, P. J.; Papworth, A. J.; Kiely, C. J.; Hutchings, G. J. *Chem. Commun.* **2002**, 2058−2059.
(4) Hughes, M. D.; Xu, Y.; Jenkins, P.; McMorn, P.; Landon, P.; Enache, D. I.; Carley, A. F.; Attard, G. A.; Hutchings, G. J.; King, F.; Stitt, E. H.; Johnston, P.; Griffin, K.; Kiely, C. J. *Nature* **2005**, *437*, 1132−1135.
(5) Fu, Q.; Saltsburg, H.; Flytzani-Stephanopoulos, M. *Science* **2003**, *301*, 935−939.
(6) Haruta, M. *Catal. Today* **1997**, *36*, 153−166.
(7) Min, B. K.; Friend, C. M. *Chem. Rev.* **1998**, *107*, 2709−2724.
(8) Chen, M.; Goodman, D. W. *Acc. Chem. Res.* **2006**, *39*, 739−746.
(9) Hashmi, A. S. K.; Hutchings, G. J. *Angew. Chem., Int. Ed.* **2006**, *45*, 7896−7936.
(10) Hutchings, G. J.; Burst, M.; Schmidbaur, H. *Chem. Soc. Rev.* **2008**, *37*, 1759−1765.
(11) Daniel, M.-C.; Astruc, D. *Chem. Rev.* **2004**, *104*, 293−346.
(12) Pyykkö, P. *Angew. Chem., Int. Ed.* **2004**, *43*, 4412−4456.
(13) Pina, C. D.; Falletta, E.; Prati, L.; Rossi, M. *Chem. Soc. Rev.* **2008**, *37*, 2077−2095.
(14) Sanchez, A.; Abbet, S.; Heiz, U.; Schneider, W.-D.; Häkkinen, H.; Barnett, R. W.; Landman, U. *J. Phys. Chem. A* **1999**, *103*, 9573−9578.
(15) Sinha, A. K.; Seelan, S.; Tsubota, S.; Haruta, M. *Top. Catal.* **2004**, *29*, 95−102.
(16) Fukuoka, A.; Dhepe, P. L. *Chem. Rec.* **2009**, *9*, 224.
(17) Corma, A.; Garcia, H. *Chem. Soc. Rev.* **2008**, *37*, 2096.
(18) Oliver-Meseguer, J.; Cabrero-Antonino, J. R.; Dominguez, I.; Leyva-Perez, A.; Corma, A. *Science* **2012**, *338*, 1452−1455.
(19) Chen, M. S.; Goodman, D. W. *Science* **2004**, *306*, 252.
(20) Turner, M.; Golvoko, V. B.; Vaughan, O. P. H.; Abdulkin, P.; Berenguer-Murcia, A.; Tikhov, M. S.; Johnson, B. F. G.; Lambert, R. M. *Nature* **2008**, *454*, 981−983.
(21) Fu, Q.; Saltsburg, H.; Flytzani-Stephanopoulos, M. *Science* **2003**, *301*, 935.
(22) Herzing, A. A.; Kiely, C. J.; Carley, A. F.; Landon, P.; Hutchings, G. J. *Science* **2008**, *321*, 1331−1335.
(23) Yoon, B.; Häkkinen, H.; Landman, U.; Wörz, A. S.; Antonietti, J.-M.; Abbet, S.; Heiz, U. *Science* **2005**, *307*, 403−407.
(24) Valden, M.; Lai, X.; Goodman, D. W. *Science* **1998**, *281*, 1647−1650.
(25) (a) Hammer, B.; Hansen, L. B.; Nørskov, J. K. *Phys. Rev. B* **1999**, *59*, 7413. (b) Nørskov, J. K.; Bligaard, T.; Hvolbaek, B.; Abild-Pedersen, F.; Chorkendorff, I.; Christensen, C. H. *Chem. Soc. Rev.* **2008**, *37*, 2163−2171.
(26) Green, I. X.; Tang, W. J.; Neurock, M.; Yates, J. T., Jr. *Science* **2011**, *333*, 736−739.
(27) Date, M.; Haruta, M. *J. Catal.* **2001**, *201*, 221−224.
(28) Date, M.; Okumura, M.; Tsubota, S.; Haruta, M. *Angew. Chem., Int. Ed.* **2004**, *43*, 2129.
(29) Landman, U.; Yoon, B.; Zhang, C.; Heiz, U.; Arenz, M. *Top. Catal.* **2007**, *44*, 145−158.
(30) (a) Comotti, M.; Pina, C. D.; Matarrese, R.; Rossi, M. *Angew. Chem., Int. Ed.* **2004**, *43*, 5812−5815. (b) Beltrame, P.; Comotti, M.; Pina, C. D.; Rossi, M. *Appl. Catal., A* **2006**, *297*, 1. (c) Comotti, M.; Pina, C. D.; Falletta, M.; Rossi, M. M. *Adv. Synth. Catal.* **2006**, *348*, 313.
(31) Fujita, T.; Guan, P.; McKenna, K.; Lang, C.; Hirata, A.; Zhang, L.; Tokunaga, T.; Arai, S.; Yamamoto, Y.; Tanaka, N.; Ishikawa, Y.; Asao, N.; Yamamoto, Y.; Erlebacher, J.; Chen, M. *Nat. Mater.* **2012**, *11*, 775−780.
(32) (a) Xu, C.; Su, J.; Xu, X.; Liu, P.; Zhao, H.; Tian, F.; Ding, Y. *J. Am. Chem. Soc.* **2007**, *129*, 42−43. (b) Jürgens, B.; Kübel, C.; Schulz, C.; Nowitzki, T.; Zielasek, V.; Biener, J.; Biener, M. M.; Hamza, A. V.; Büumer, M. *Gold Bull.* **2007**, *40*, 142−149. (d) Zielasek, V.; Jürgens, B.; Schulz, C.; Biener, J.; Biener, M. M.; Hamza, A. V.; Baümer, M. *Angew. Chem., Int. Ed.* **2006**, *45*, 8241−8244. (e) Sanchez-Castillo, M. A.; Couto, C.; Kim, W. B.; Dumesic, J. A. *Angew. Chem., Int. Ed.* **2004**, *43*, 1140−1142.
(33) Review about the catalytic activity of unsupported gold nanoparticles: Mikami, K.; Dhakshinamoorthy, A.; Alvaro, M.; Garcia, H. *Catal. Sci. Tech.* **2013**, *3*, 58−69.
(34) Gao, Y.; Shao, N.; Bulusu, S.; Zeng, X. C. *J. Phys. Chem. C* **2008**, *112*, 8234−8238.
(35) (a) Lopez, N.; Nørskov, J. K. *J. Am. Chem. Soc.* **2002**, *124*, 11262−11263. (b) Remediakis, I. N.; Lopez, N.; Nørskov, J. K. *Angew. Chem., Int. Ed.* **2005**, *44*, 1824−1826.
(36) Bongiorno, A.; Landman, U. *Phys. Rev. Lett.* **2005**, *95*, 106102.
(37) (a) Molina, L. M.; Hammer, B. *Appl. Catal., A* **2005**, *291*, 21−31. (b) Molina, L. M.; Rasnussen, M. D.; Hammer, B. *J. Chem. Phys.* **2004**, *120*, 7673−7680. (c) Molina, L. M.; Hammer, B. *J. Catal.* **2005**, *233*, 399−404.
(38) Socaciu, L. D.; Hagen, J.; Bernhardt, T. M.; Woste, L.; Heiz, U.; Häkkinen, H.; Landman, U. *J. Am. Chem. Soc.* **2003**, *125*, 10437−10455.
(39) (a) Rodriguez, J. A.; Feria, L.; Jirsak, T.; Takahashi, Y.; Nakamura, K.; Illas, F. *J. Am. Chem. Soc.* **2010**, *132*, 3177−3186. (b) Roldán, A.; Ricart, J. M.; Illas, F.; Pacchioni, G. *J. Phys. Chem. C* **2010**, *114*, 16973−16978. (c) Roldán, A.; González, S.; Ricart, J. M.; Illas, F. *ChemPhysChem* **2009**, *10*, 348−351.
(40) (a) Gao, Y.; Shao, N.; Pei, Y.; Chen, Z.; Zeng, X. C. *ACS Nano* **2011**, *5*, 7818−7829. (b) Gao, Y.; Zeng, X. C. *ACS Catal.* **2012**, *2*, 2614−2621. (c) Li, H.; Pei, Y.; Zeng, X. C. *J. Chem. Phys.* **2010**, *133*, 134707.
(41) Li, H.-J.; Ho, J.-J. *J. Phys. Chem. C* **2008**, *112*, 8234−8238.
(42) Wang, F.; Zhang, D.; Xu, X.; Ding, Y. *J. Phys. Chem. C* **2009**, *113*, 18032−18039.
(43) Molina, L. M.; Lesarri, A.; Alonso, J. A. *Chem. Phys. Lett.* **2009**, *468*, 201−204.
(44) Chen, G.; Li, S. J.; Su, Y.; Wang, V.; Mizuseki, H.; Kawazoe, Y. *J. Phys. Chem. C* **2011**, *115*, 20168−20174.
(45) Stamatakis, M.; Christiansen, M. A.; Vlachos, D. G.; Mpourmpakis, G. *Nano Lett.* **2012**, *12*, 3621−3626.
(46) (a) Kim, H. Y.; Li, H. M.; Henkelman, G. *J. Am. Chem. Soc.* **2012**, *134*, 1560−1570. (b) Kim, H. Y.; Henkelman, G. *J. Phys. Chem. Lett.* **2012**, *2*, 2194−2199.
(47) Wallace, W. T.; Whetten, R. L. *J. Phys. Chem. B* **2000**, *104*, 10964−10968.
(48) Veldeman, N.; Lievens, P.; Andersson, M. *J. Phys. Chem. A* **2005**, *109*, 11793−11801.
(49) Fielicke, A.; Helden, G.; Meijer, G.; Simard, B.; Rayner, D. M. *J. Phys. Chem. B* **2005**, *109*, 23935−23940.
(50) Wallace, W. T.; Whetten, R. L. *J. Am. Chem. Soc.* **2002**, *124*, 7499−7505.
(51) Hagen, J.; Socaciu, L. D.; Elijazyfer, M.; Heiz, U.; Bernhardt, T. M.; Wöste, L. *Phys. Chem. Chem. Phys.* **2002**, *4*, 1707−1709.
(52) Boccuzzi, F.; Chiorino, A. *J. Phys. Chem. B* **2000**, *104*, 5414−5416.
(53) Hagen, J.; Socaciu, L. D.; Heiz, U.; Bernhardt, T. M.; Woste, L. *Eur. Phys. J. D* **2003**, *24*, 327.
(54) Zhai, H.-J.; Wang, L.-S. *J. Chem. Phys.* **2005**, *122*, 051101.
(55) Fielicke, A.; Helden, G.; Meijer, G.; Pedersen, D. B.; Simard, B.; Rayner, D. M. *J. Am. Chem. Soc.* **2005**, *127*, 8416−8427.
(56) Socaciu, L. D.; Hagen, J.; Bernhardt, T. M.; Woste, L.; Heiz, U.; Hakkinen, H.; Landman, U. *J. Am. Chem. Soc.* **2003**, *125*, 10437−10445.
(57) Zhai, H.-J.; Kiran, B.; Dai, B.; Li, J.; Wang, L.-S. *J. Am. Chem. Soc.* **2005**, *127*, 12098−12106.
(58) Zhai, H.-J.; Pan, L.-L.; Dai, B.; Kiran, B.; Li, J.; Wang, L.-S. *J. Phys. Chem. C* **2008**, *112*, 11920−11928.
(59) Pal, R.; Huang, W.; Wang, Y.-L.; Hu, H.-S.; Bulusu, S.; Xiong, X.-G.; Li, J.; Wang, L.-S.; Zeng, X. C. *J. Phys. Chem. Lett.* **2011**, *2*, 2288−2293.
(60) Bürgel, C.; Reilly, N. M.; Johnson, G. E.; Mitrić, R.; Kimble, M. L.; Castleman, A. W., Jr.; Bonacić-Koutecký, V. *J. Am. Chem. Soc.* **2008**, *130*, 1694−1698.
(61) Xie, Y.; Dong, F.; Bernstein, E. R. *Catal. Today* **2011**, *177*, 64−71.
(62) Aguilar-Guerrero, V.; Gates, B. C. *Catal. Lett.* **2009**, *130*, 108−120 and references therein.

(63) Aguilar-Guerrero, V.; Gates, B. C. *J. Catal.* **2008**, *260*, 351−357.
(64) Hartshorn, H.; Pursell, C. J.; Chandler, B. D. *J. Phys. Chem. C* **2009**, *113*, 10718−10725.
(65) Diemant, T.; Hartmann, H.; Bansmann, J.; Behm, R. J. *J. Catal.* **2007**, *252*, 171−177.
(66) Diemant, T.; Zhao, Z.; Rauscher, H.; Bansmann; Behm, R. J. *Top. Catal.* **2007**, *44*, 83.
(67) Menegazzo, F.; Manzoli, M.; Chiorino, A.; Boccuzzi, F.; Tabakova, T.; Signoretto, M.; Pinna, F.; Pernicone, N. *J. Catal.* **2006**, *237*, 431−434.
(68) Meier, D. C.; Bukhtiyarov, V.; Goodman, D. W. *J. Phys. Chem. B* **2003**, *107*, 12668−12671.
(69) Derrouiche, S.; Gravejat, P.; Bianchi, D. *J. Am. Chem. Soc.* **2004**, *126*, 13010−13015.
(70) Wong, K.; Zeng, Q.; Yu, A. *Chem. Eng. J.* **2009**, *155*, 824−828.
(71) Rodriguez, P.; Koverga, A. A.; Koper, M. T. M. *Angew. Chem., Int. Ed.* **2010**, *49*, 1241−1243.
(72) Rodriguez, P.; Kwon, Y.; Koper, M . T. M. *Nature Chem.* **2012**, *4*, 177−182.
(73) Xing, X.; Yoon, B.; Landman, U.; Parks, J. H. *Phys. Rev. B* **2006**, *74*, 165423.
(74) Yoon, B.; Koskinen, P.; Huber, B.; Kostko, B.; Issendorff, B. v.; Häkkinen, H.; Moseler, M.; Landman, U. *ChemPhysChem* **2007**, *8*, 157−161.
(75) Bulusu, S.; Li, X.; Wang, L. S.; Zeng, X. C. *Proc. Natl. Acad. Sci. U.S.A.* **2006**, *103*, 8326−8330.
(76) Shao, N.; Huang, W.; Gao, Y.; Wang, L. M.; Li, X.; Wang, L. S.; Zeng, X. C. *J. Am. Chem. Soc.* **2010**, *132*, 6596−6605.
(77) Bulusu, S.; Li, X.; Wang, L. S.; Zeng, X. C. *J. Phys. Chem. B* **2007**, *111*, 4190−4198.
(78) Perdew, J. P.; Burke, K.; Ernzerhof, M. *Phys. Rev. Lett.* **1996**, *77*, 3865−3868.
(79) Tao, J. M.; Perdew, J. P.; Staroverov, V. N.; Scuseria, G. E. *Phys. Rev. Lett.* **2003**, *91*, 146401.
(80) (a) Delley, B. *J. Chem. Phys.* **1990**, *92*, 508−517. (b) Delley, B. *J. Chem. Phys.* **2000**, *113*, 7756−7764.
(81) Frisch, M. J. et al.. *Gaussian 09, revision A.01*; Gaussian, Inc., Wallingford, CT, 2009.
(82) Zhang, C.; Yoon, B.; Landman, U. *J. Am. Chem. Soc.* **2007**, *129*, 2228−2229.
(83) Chris Harding, C.; Habibpour, V.; Kunz, S.; Farnbacher, A. N.; Heiz, U.; Yoon, B.; Landman, U. *J. Am. Chem. Soc.* **2009**, *131*, 538−548.
(84) Li, H.; Pei, Y.; Zeng, X. C. *J. Chem. Phys.* **2010**, *133*, 134707.
(85) Huang, W.; Wang, L.-S. *Phys. Rev. Lett.* **2009**, *102*, 153401.
(86) Huang, W.; Ji, M.; Dong, C.-D.; Gu, X.; Wang, L.-M.; Gong, X. G.; Wang, L.-S. *ACS Nano* **2008**, *2*, 897−904.
(87) Long, C. G.; Gilbertson, J. D.; Vijayaraghavan, G.; Stevenson, K. J.; Pursell, C. G.; Chandler, B. D. *J. Am. Chem. Soc.* **2008**, *130*, 10103−10105.
(88) Yoon, B.; Hakkinen, H.; Landman, U. *J. Phys. Chem. A* **2003**, *107*, 4066−6071.
(89) Janssens, T. V. W.; Clausen, B. S.; Hvolbaek, B.; Falsig, H.; Christensen, C. H.; Bligaard, T.; Nørskov, J. K. *Top. Catal.* **2007**, *44*, 15−26.
(90) Mavrikakis, M.; Stoltze, P.; Nørskov, J. K. *Catal. Lett.* **2000**, *64*, 101−106.
(91) Salisbury, B. E.; Wallace, W. T.; Whetten, R. L. *Chem. Phys.* **2000**, *262*, 131−141.
(92) Pal, R.; Wang, L.-M.; Pei, Y.; Wang, L.-S.; Zeng, X. C. *J. Am. Chem. Soc.* **2012**, *134*, 9438−9444.
(93) Chang, C.-R.; Wang, Y.-G.; Li, J. *Nano Res.* **2011**, *4*, 131−142.
(94) Liu, Z.-P.; Hu, P.; Alavi, A. *J. Am. Chem. Soc.* **2002**, *134*, 14770−14779.
(95) Wang, C.-M.; Fan, K.-N.; Liu, Z.-P. *J. Am. Chem. Soc.* **2007**, *129*, 2642−2647.
(96) Lippert, G.; Hutter, J.; Parrinello, M. *Mol. Phys.* **1997**, *92*, 477.
(97) Goedecker, S.; Teter, M.; Hutter, J. *Phys. Rev. B* **1996**, *54*, 1703.
(98) Hartwigsen, C.; Goedecker, S.; Hutter, J. *Phys. Rev. B* **1998**, *58*, 3641 (GTH).
(99) The CP2K developers group, http://cp2k.berlios.de/, 2004.
(100) Pei, Y.; Shao, N.; Gao, Y.; Zeng, X. C. *ACS Nano* **2010**, *4*, 2009−2020.
(101) Gao, Y.; Shao, N.; Pei, Y.; Zeng, X. C. *Nano Lett.* **2010**, *3*, 1055−1062.
(102) Gao, W.; Chen, X. F.; Li, J. C.; Jiang, Q. *J. Phys. Chem. C* **2010**, *114*, 1148−1153.